Inflow dynamics in weakly stratified lakes subject to large isopycnal displacements

C. L. Ramón[1,2], M. C. Priet-Mahéo[1,3], F. J. Rueda[2], and H. Andradóttir[1]

[1] Faculty of Civil and Environmental Engineering, University of Iceland, Hjardarhagi 2-6, IS107 Reykjavík, Iceland. Emails: mcc1@hi.is and hrund@hi.is.

[2] Department of Civil and Environmental Engineering and Water Research Institute, University of Granada, Spain. Emails: crcasanas@ugr.es and fjrueda@ugr.es.

[3] Icelandic Meteorological Office, Bústaðavegur 7-9, IS 108 Reykjavík, Iceland

Corresponding authors: H. Andradóttir (hrund@hi.is), C. L. Ramón (crcasanas@ugr.es)

Key Points:

- Large-amplitude isopycnal displacements can strongly affect river intrusion depths in weakly stratified lakes
- Strong downwelling near the inlet promotes metalimnetic river intrusions while strong upwelling, bottom intrusions in the near field
- Basin scale internal circulation can either accelerate or decelerate lateral transport across lake depending on wind direction

Abstract

The effect of large-amplitude isopycnal displacements, frequently observed in deep medium-size arctic lakes during the ice-free period, on the near- and far-field fate of negatively buoyant river inflows is explored in this work. A three-dimensional transport and hydrodynamic model of sub-arctic Lake Lagarfljót was used to simulate the fate of river inflows during the summer stratification period. The intrusion dynamics are strongly affected by the amplitude and direction (downwelling/upwelling) of the isopycnal displacements induced by the wind near the river inlet. These displacements control the distance of travel of the river plume until reaching the layers with maximum density gradients (pycnocline) and, thus, the mixing ratio between the river plume and the lake water. Specifically, strong upwelling near the inlet causes the river to flow to the bottom as an underflow. Under downwelling, river plumes tend to form metalimnetic intrusions. The influence of the isopycnal displacements on the initial river fate can be parameterized using a time-varying density Richardson number, which needs to be smoothed to account for the effects of unsteadiness. Large amplitude internal motions, of up to 70 m in Lake Lagarfljót, move deep underflows upwards to shallower basins where they could be readily incorporated into the surface mixed layer and rapidly flushed out of the lake. Metalimnetic currents associated with the V2H1 internal circulation can also accelerate riverine transport out of the lake.

1 Introduction

River inflows are the main source of nutrients, organic material, and suspended sediments for lakes and reservoirs (Ford and Johnson, 1986; Dallimore et al. 2003; Morillo et al., 2008). The effects of rivers on the biogeochemistry of these systems largely depend on the fate of the river plumes (e.g., MacIntyre et al., 2006), that is whether they intrude within the surface, intermediate or deeper layers of the lake. River plumes will remain near the surface, forming overflows, if their density is lower than the density of the surface layer (Chen, 1980; Luketina and Imberger, 1987; Cáceres et al., 2002). They will plunge and flow downward along the bottom, in turn, if they are negatively buoyant. In that case, they will flow as gravity currents, entraining ambient fluid from above, until reaching the lake bottom as underflows (Hebbert et al., 1979; Finger et al., 2006). In the case of stratified lakes, they might separate from the bottom and flow horizontally as intrusions (interflows) if they encounter layers with similar densities above the lake bottom (Stevens et al., 1995; Ahlfeld et al., 2003; Finger et al., 2006). Our understanding of the near field fate of river plumes is largely derived from quiescent receiving bodies. This includes laboratory experiments (Ellison and Turner, 1959; Alavian et al., 1992; Hallworth et al., 1996); numerical simulations (Chung and Gu, 1998; Bournet et al., 1999; Kassem et al., 2003); and field experiments in lakes and reservoirs (e.g. Fischer and Smith, 1983; Hebbert et al., 1979; Dallimore et al., 2001). Lakes, though, are dynamic systems (Imberger, 1998; Imberger and Patterson, 1990), where motions in the ambient water may exert a strong influence on the behavior of river plumes, as recently shown, for example, by Hogg et al. (2018) and Ouillon et al. (2019) in their laboratory and numerical experiments, respectively. They demonstrated that large amplitude internal waves can, in fact, interact with down-slope gravity currents, causing significant reductions of both the mass transport by the gravity current and its thickness.

High-latitude lakes, located near or above the Arctic Circle, are an example of such dynamic systems. Subject to low solar insolation, cold and wet weather, and strong wind forcing, these lakes tend to exhibit weak water-column stability and experience frequent and long-lasting upwelling events (see Priet-Mahéo et al., 2019). Given the large amplitude of the isopycnal displacements occurring in (sub-) arctic systems, we hypothesize that the initial fate of negatively buoyant river plumes, whether they form interflows or underflows, could vary depending on the amplitude and direction (downwelling-upwelling) of those displacements near

the inlet at the time of the inflow (see conceptual model in Fig. 1). The above hypothesis can be extended to strong wind events in large temperate lakes prior to and after the summer stratification, when the water column is weakly stratified (e.g., Engelhardt and Kirillin, 2014). In a quiescent, two-layer basin, a pulse of negatively buoyant river water parcel may become a metalimnetic intrusion (interflow), or, in turn, it will reach the bottom of the lake as an underflow, depending on the level of mixing and entrainment occurring before the plume reaches the pycnocline (H). If the entraining plume density, once it reaches the pycnocline, exceeds that of the hypolimnion, it will cross the density step and travel to the bottom. If not, it will separate at the pycnocline, and become an interflow. If severe downwelling occurs near the inlet of a large lake (Fig. 1b), and these conditions hold for the time a pulse of river water needs to reach the pycnocline, the distance L over which the plume can entrain lighter fluid (hence the mixing ratio at the pycnocline) will increase drastically (by ΔL in Fig. 1b). Note that the distance of travel relates to H as $L \sim H\,(1/I^2+1)^{0.5}$, being I the lake bottom slope. As a result, a river pulse that would have entered as an underflow in a quiescent basin may enter as an interflow because of a longer trajectory for entrainment, more effective mixing and entrainment with light ambient water. Conversely, the same negatively buoyant river plume (pulse) may enter the lake as an underflow (Fig. 1c), when the pycnocline rises near the inflow, even reaching the surface, and the distance from the surface to the hypolimnion becomes short (e.g., $L = 0$ in Fig 1c). Note that the term "displacements" is here used to refer to isopycnal tilts forced either by wind or resulting from free internal waves. In this study, we focus on long-period free internal waves or on equilibrium tilts developing in response to direct wind-forcing, so that quasi-steady state conditions can be assumed for each riverine pulse.

To the extent of our knowledge, the behavior of river plumes in weakly stratified lakes subject to large amplitude isopycnal displacements remains largely unexplored. Our goal is to assess the effect of the latter on the initial (and to a lesser extend far field) fate of river plumes. For this purpose, we use sub-arctic Lake Lagarfljót (Fig. 2), characterized by the development of a weak stratification in summer and the occurrence of highly-turbid river inflows of glacial origin in its southern end. In this lake, the internal dynamics are largely driven by the wind with frequencies that mimic those of the external forcing (forced internal oscillations), as indicated by the results of Priet-Mahéo et al. (2019). The paper is organized as follows. First, the modeling methods, theoretical framework and analyses are presented. Then, the evolving lake

stratification, wind forcing and the fate of the river inflows are described. Finally, the mechanisms by which internal motions control the fate of river plumes near and far from the inlet of weakly stratified lakes are analyzed.

2 Methods

2.1 ***Approach –*** Our work is based on the analysis of the three-dimensional simulation of transport and mixing processes in Lake Lagarfljót during the thermal stratification period in the summer of 2009. This simulation (here referred to as "reference") is the same presented and discussed in Priet-Mahéo et al. (2019; see their results and model validation). Our working hypothesis was formulated after a detailed analysis of the results of this reference simulation and field measurements (Priet-Mahéo, 2019). Then, a simulation was conducted in which the direction of the wind forcing was rotated 180° (rotated wind-run), such that the phase of the internal oscillations at the time of the major inflow events were opposite to those in the reference simulation. Our analyses are based on the interpretation of the results of a series of simulations of pulse-release tracer experiments conducted with the velocity fields from those two sets of simulations (reference and rotated-wind). In each experiment, the evolution of the tracer plumes in the lake is analyzed.

2.2 ***Study site*** - Lake Lagarfljót is a medium size (27 km long, 2 km wide), deep (110 m) fjord-type lake oriented in the SW-NE direction at 65°N in North-Eastern Iceland (Fig. 2). Two sub-basins are separated by a ca. 30-m deep sill. The larger sub-basin to the South of the constriction is 20 km long, and has a maximum depth of 110 m. The northern N-basin is 7 km long and is shallower than the S-basin, with a maximum depth of 42 m. The average hydraulic residence time of water in the lake is 0.5 years. The largest inflow into Lake Lagarfljót occurs through a unique and wide channel in the southernmost end of the lake. This channel carries water from three different sources: (1) the glacial river Jökulsá í Fljótsdal; (2) its non-glacial tributaries Kelduá and Fellsá; and (3) water diverted from Hálslón reservoir, regulating the flow from a series of glacial rivers draining a neighboring watershed, through the Kárahnjúkar power plant. The glacial rivers contain high concentration of fine clay and silt sediments, rendering the

lake a greenish-greyish color. The major non-glacial tributary to the lake is river Grímsá that enters the N-basin (Fig. 2).

2.3 ***Hydrodynamic and transport model of Lake Lagarfljót*** - Simulations were conducted with a modified version of the 3D, z-coordinate, hydrostatic transport and mixing model of Smith (2006), in which the contribution of suspended sediment concentration, C_{SS}, to water density is accounted for. The contribution of suspended solids, $\Delta\rho_{ss}$, to fluid density was estimated as follows (Ford and Johnson, 1983):

$$\rho(T, C_{ss}) = \rho_T + \Delta\rho_{SS} = \rho_T + \left(1 - \frac{1}{SG}\right) C_{ss} \quad (1)$$

where units of C_{SS} are in (kg m^{-3}) and the nonlinear equation of state of Chen and Millero (1986) was used to estimate the contribution of temperature to water density (ρ_T). The specific gravity SG of glacial till was taken as 2.7 based on measurements by Pálsson and Vilmundardóttir (2003). Particle settling was assumed negligible following Striberger et al. (2011), who argued that most of the sediments or rock flour brought by Jökulsá í Fljótsdal stays in suspension in the water in the summer and deposit during the winter. These assumptions were further supported by model results at the lake outflows which reproduce the evolution of the C_{SS} signal measured at this site (RMSE =0.011 kg m^{-3} and Fig. A1 in Priet-Mahéo et al. 2019). By neglecting particle settling in the simulations, convective sedimentation (e.g., Jazi and Wells, 2020) is not accounted for. Convective sedimentation could indeed be important at the time of the numerical tracer experiments (days 190-280), but only locally, once the negatively buoyant river plumes, loaded with particles, detach from the lake bottom and intrude at intermediate depths where turbulence levels fade out. Despite this potential limitation, the model is able to correctly reproduce the thermal structure in the lake. Model results were validated against temperature data collected by three thermistor chains deployed in the south, center and north of the lake south basin (see details in the Supporting Information of Priet-Mahéo et al. 2019). Average root mean square errors between model and field data ranged from 0.45ºC to 0.52ºC. The model domain discretization and hydrometeorological input data from the Icelandic Meteorological Office, Landsvirkjun (National Power Company of Iceland) and Orkusalan are described in Appendix A.

157 The stair-like representation of slopes in z-coordinate models induces grid convective
158 mixing as the underflows move to the bottom of the lake (e.g., Winton et al., 1998; Legg et al.,
159 2006). To evaluate the relevance of this extra source of numerical mixing, the grid resolution
160 used for lake Lagarfljót was also tested against the theoretical and laboratory-based
161 parameterization of intrusion depths for river plumes entering a linearly stratified lake by Wells
162 and Nadarajah (2009). The model predicted intrusion depths that were within the range of
163 variability observed in the laboratory (see details of these simulations in Appendix B).

164 2.4 ***River plume monitoring and characterization*** - Tracer-pulse release experiments
165 were used to characterize the fate of river inflows. Each experiment consisted of a release of a
166 pulse (one hour) of a tracer with a concentration of 100 units at the inflow section, each day
167 during the stratified period starting at 7:00h on day 190 and ending at 7:00 h on day 280. Within
168 this period, nonlinear effects of temperature on water density (i.e. cabbeling, e.g., Carmack 1978)
169 are not in control of the lake-river dynamics (see section 4.1). The extension of the plume was
170 tracked during the 5-day period immediately after the release, as the group of cells in the 3D-
171 tracer field with concentrations ≥ 0.05 units. The weighted-average characteristic of the plume at
172 any given time *t* within the 5-day period was estimated as follows:

173

174 $$\underline{\theta}(t) = \frac{\sum_{i=1}^{n(t)} \theta_i(t) C_i(t)}{\sum_{i=1}^{n} C_i(t)} \qquad (2)$$

175

176 Here n is the total number of cells within the plume (i.e. its spatial extent)*;* i is the cell number;
177 C_i its tracer concentration*,* and θ_i represents the property of interest. Properties characterized
178 included water temperature, C_{SS}, and location (x, y, and z) of the plume. Note that n, θ_i and C_i are
179 a function of time.

180 The time-varying magnitude of the average plume depth, calculated with Eq. 2, was used
181 to estimate the depth when a plume stops descending for the first time (t_{ID}). This represents the
182 depth at which a plume separates from the bottom to form an intrusion, and will be referred to as
183 the separation depth, *SD*. The plume properties at that time t_{ID} (its temperature T_{ID}, suspended

184 solid concentration $C_{SS\text{-}ID}$, and density ρ_{ID}) were calculated. The depth in the background density
185 profile where the density equals ρ_{ID} was referred to as the equilibrium intrusion depth (ID_E).The
186 background density was estimated by sorting the simulated instantaneous 3D density fields using
187 a similar sorting algorithm as laid out in Rueda and Schladow (2009) (see also Winters et al.,
188 1995). The theoretical intrusion depth, ID_0, of the plume was estimated as the depth in the
189 background density profile where the density equals that of the river at the inlet, ρ_0. The
190 difference between ID_E and SD accounts for the effects of the isopycnal displacements on
191 intrusion dynamics. The difference between ID_E and the theoretical intrusion depth, ID_0, in turn,
192 accounts for the effects of mixing between river and lake water.

193 The mixing ratio for any given plume at the separation point was calculated as:

194

195 $$\gamma = (\rho_0\text{-}\rho_1)/(\rho_{ID}\text{-}\rho_1) \quad (3)$$

196

197 where ρ_1 and ρ_2 are the surface and hypolimnetic densities of the lake, respectively. It will be
198 assumed that the stratification can be described as consisting of two-layers. The epilimnion in the
199 density profiles was identified following Priet-Mahéo et al. (2019), as the layer where densities
200 differ at most 0.03 kg m^{-3} from the surface density. Similarly, the hypolimnion was taken as the
201 layer where densities differ at most 0.03 kg m^{-3} from bottom densities. The depth of the
202 pycnocline H was taken midway between the bottom of the epilimnion and the top of the
203 hypolimnion.

204

205 **3 Theoretical framework for initial river fate**

206 Wells and Wettlaufer (2007, see also Forrest et al., 2008) suggest that whether a negatively
207 buoyant inflow of density ρ_0 detaches and forms an intrusion or penetrates the density step to
208 reach the bottom, can be parameterized in terms of the density Richardson number Ri_ρ, defined
209 as

210

$$Ri_\rho = g'_{12}\frac{H}{B_0^{2/3}} \quad (4)$$

Here $g'_{12} = g\,(\rho_2 - \rho_1)/\,\rho_1$ is the reduced gravity of the ambient water density step and B_0 is the inflow buoyancy flux per unit width of the gravity current. The buoyancy flux, in turn, is calculated as $g'_0 Q_0/W$, from the inflow reduced gravity $g'_0 = g\,(\rho_0 - \rho_1)/\,\rho_1$, the width W, and the river flow rate Q_0. This form of the Richardson number compares the density excess of the river plume after entrainment and once it reaches the interface, in relation to the density contrast across that interface. If Ri_ρ exceeds a critical value Ri_ρ^*, the gravity current forms an interflow at the density step, and by contrast, if $Ri_\rho << Ri_\rho^*$, it will penetrate through the density step forming an underflow. For $Ri_\rho \approx Ri_\rho^*$, part of the gravity current flowing into the density step would leak to the bottom, as an underflow, and form multiple intrusions (Wells and Wettlaufer, 2007). Note that this criterion is only applicable to negatively buoyant plumes, for which $\rho_0 > \rho_2$. Otherwise, independently of the entrainment in the upper layer and the value of Ri_ρ, the gravity current will also develop metalimnetic intrusions. This framework has been verified by field and laboratory experiments in strongly stratified systems where the isopycnals were horizontal and the water nearly quiescent (Cortés et al., 2014a, 2014b and 2015). The critical value Ri_ρ^* is slope-dependent (Wells and Wettlaufer, 2007). Existing estimates of Ri_ρ^* are of O(1-10), varying between studies. For example, $Ri_\rho^* \sim$ 21-27 in the laboratory experiments reported by Wells and Wettlaufer (2007), with bottom slopes ranging from 30° to 90°. Cortés et al. (2014b) reported values of $Ri_\rho^* \sim$ 42-75, with 25° slopes. Tanimoto et al. (2020) reported values of Ri_ρ^* of ca. 3.5 in their experiments with bottom slopes of 6°.

We propose to adapt the theoretical framework of Wells and Wettlaufer (2007) to explain the effect of the slow, large-amplitude isopycnal displacements on the initial fate of negatively buoyant river plumes in arctic water systems (Fig. 1b-c). Together with the two-layer stratification assumption, it will be assumed that the effect of wind forcing on the intrusion dynamics is primarily driven by the rising and lowering of the pycnocline near the inlet. Surface mixing will be assumed to have a negligible effect on the inflow dynamics during the course of any given wind event. This assumption is based on the earlier results of Priet-Mahéo et al. (2019) in their study of Lake Lagarfljót. They showed that the rate of work imparted by wind during

summer stratification in Lagarflót was largely used to energize large scale isopycnal displacements, being the fraction in large-scale mixing significantly lower. It will also be assumed that the duration of the wind event is longer than one quarter of the first mode internal-wave period (so that the equilibrium tilt of the internal structure is reached) and, also, exceeds the travel time to the pycnocline. This is the case in Lake Lagarfljót where wind events frequently last more than 24 h, which is ca. one quarter of the V1H1 mode period (Fig. 3a and analysis in Priet-Mahéo et al. (2019)). Under those assumptions we can analyze the inflow dynamics as being in quasi-steady state and define a time variable density Richardson number,

$$Ri_\rho = g'_{12}\frac{H(t)}{B_0^{2/3}} = g'_{12}\frac{H_{bck}+\Delta H(t)}{B_0^{2/3}} = Ri_{\rho-bck} + \Delta Ri_\rho \quad (5)$$

where, instead of using a constant H, as in Wells and Wettlaufer (2007), we use a time variable displacement $H(t)$ to account for the oscillatory nature of the pycnocline in the near-field. Here, H_{bck} is the pycnocline depth at equilibrium, and $\Delta H(t)$ represents the internal displacements. The first component of Ri_ρ will be referred to as background density Richardson number $Ri_{\rho\text{-}bck}$. The second component, ΔRi_ρ, accounts for the effects of the internal oscillations. In this framework, changes in the intrusion dynamics will occur in response to internal oscillations, at any given time, if the predicted behavior of the plume using the $Ri_{\rho\text{-}bck}$ differs from that predicted using the time variable Ri_ρ, i.e.

$$\mathrm{sgn}\left(Ri_{\rho-bck} - Ri_\rho^*\right) \neq \mathrm{sgn}\left(Ri_\rho - Ri_\rho^*\right) \quad (6)$$

Note that, the effects of isopycnal displacements driven either by wind events or free-internal waves are filtered out in the calculation of $Ri_{\rho\text{-}bck}$, but $Ri_{\rho\text{-}bck}$ may still change as a result of seasonal or synoptic scale mixing.

4 Results and Discussion

4.1 ***Hydro-meteorological forcing and lake stratification*** **–** Forcing records for Lake Lagarfljót during the study period are shown in Fig. 3. Winds were strong, with daily-averages as high as 9 m s^{-1} (Fig. 3a), and predominantly from the north (negative values for the wind velocities along the lake thalweg shown in Fig. 3a). Low insolation (Fig. 3d), cold (Fig. 3b) and wet weather (Figs. 3c) typically occurred during periods of strong northerly and north-easterly winds (see also Hanna et al., 2004; Crochet et al., 2007; Jónsdóttir and Uvo, 2009). Dry and warm weather, in turn, prevailed during periods of southerly winds (see for example, the events around day 205, 216-220 or 250-260). Southern inflow rates and densities varied on a seasonal and, more importantly, on a synoptic basis (Fig. 3e). Volumetric flows decreased from an average of 200 $m^3 s^{-1}$ in June (days <181) to an average of 120 $m^3 s^{-1}$ in October (days > 274), while the density increased by ≈ 0.2 kg m^{-3}. Inflow events, lasting 5-10 days, discharged up to 280 $m^3 s^{-1}$. Inflow events during predominantly southerly wind (for example on days 217 and 256) coincided with increases in air temperature (Fig. 3b), and were likely related to melting of the glaciers and snow cover in the upstream part of the southern-inflow catchment area. Events during northerly winds (days 231, 236-240), however, coincided with the passage of low-pressure systems carrying colder air and rainfall. During all discharge events the river temperature increased weakly (ca. 1-2 $^{\circ}$C, Fig. 3f). In June, when suspended sediment concentrations remained moderate, the river density dropped considerably during the melting events (see for example day 180 in Fig. 3e). In the consecutive events in August (days 217-260), however, the suspended sediment load increased with discharge to values that were triple the summer base-flow (Fig. 3f). This in turn raised substantially the density of the entering river (Fig. 3d). The increase in suspended sediments is a distinctive signature of the river water and can be used to trace its fate in the lake. From day 230 onwards (except at peak flows) the temperature of the southern inflow decreased to values below the temperature of maximum density (~ 3.98 °C), but the suspended sediment load also increased (C_{SS} > 0.2 kg m^{-3}) and controlled the lake-river density difference.

Seasonal and depth variations of water density in Hafursá, near the deepest site of the lake (Fig. 2), together with the corresponding changes in water temperature and suspended sediment concentration are shown in Figs. 4a-c. Note first the weak density changes occurring in depth, with a maximum top-bottom density difference of 0.3 kg m^{-3} (Fig. 4a). Maximum top-

297 bottom temperature differences do not exceed 6 ˚C in the 110 m of water column, even at the
298 time of maximum stratification in August (days 213-243, Fig. 4b). Gradients in the concentration
299 of suspended sediments (Fig. 4c) started forming in the lake at mid-depth at a similar time as
300 water temperature, and progressed towards the bed, persisting there longer than temperature
301 gradients.

302

303 4.2 ***Initial fate of river plumes*** – In weakly stratified systems even small changes in river
304 temperatures or suspended sediment loads have the potential to generate large changes in
305 intrusion depths. The evolution of the theoretical intrusion depth (see gray thick line, in Fig. 4c)
306 suggests, for example, that the river would form alternatively over- and under-flows in the
307 absence of mixing during early spring when the stratification starts to develop, as a result of even
308 moderate changes in river temperature. After the river suspended sediment load starts increasing
309 (after day 180), and the stratification develops, the inflows become negatively buoyant and,
310 according to its theoretical intrusion depth, should form mostly underflows. However, our
311 reference simulation suggests that elevated suspended sediment concentrations develop in the
312 metalimnion between 20 and 50 m below the free surface (Fig. 4c) after day 180, which suggests
313 that river plumes formed metalimnetic intrusions. The largest densities in the river occurred
314 during the inflow events (Fig. 3e), when the suspended sediment concentrations in the river and,
315 hence, its density increased abruptly. From their ID_0, one would expect that the river plumes
316 during those events would flow to the bottom as underflows. However, this is not the case, for
317 example, during the inflow event of day 236-240 with northerly winds, when the river enters the
318 lake at 50-m depth as an interflow (see also Fig. 5a). By contrast, during the inflow event on
319 days 256-260 with southerly winds, the negative buoyant river flows to reach the bottom (Fig.
320 5b).

321 These results suggest that the fate of river plumes in the near-field may, indeed, vary, as
322 hypothesized, depending on the upwelling/downwelling direction of the isopycnal displacements
323 at the time when inflows occur. Interflows will tend to occur when the isopycnals downwell in
324 the southern end (Fig. 1b). Underflows, in turn, will tend to occur under strong upwelling
325 conditions near the inlet (Fig. 1c). The fact that the direction of the isopycnal displacements
326 appears to have some influence on the fate of river plumes in the near field is further supported

by comparing the results of the simulation with rotated wind against those of the reference run. As the tilt of the isopycnals near the inlet is reversed with wind blowing from the opposite direction, the river plume changes its behavior from an interflow to an underflow, and vice versa (compare Figs. 5a,c and Fig. 5b,d, and see Fig. 4d). Note that the vertical distribution of suspended sediment concentrations in Hafursá in the simulation with the rotated winds are significantly different (compare Figs. 4c,d), in particular, during the inflow events of days 236-240 and 256-260.

4.3 ***Internal dynamics and river plume mixing ratios*** – Implicit in our working hypothesis, is that any change in the depth of the isopycnals occurring near the inlet (in response to wind-driven or free internal oscillations) will cause significant changes in the mixing ratio between gravity currents and lake water at the separation point. In Fig. 6 we have plotted the mixing ratio (Eq. 3) for each of the tracer pulse experiments in the reference and rotated-wind simulations, against the depth of the pycnocline and the travel distance L at the time of the tracer injection. Median values for the mixing ratios are 2.4 and 1.5 for the reference and rotated-wind runs, respectively (Table 1). These values are similar to those reported in the literature. For example, Hogg et al. (2013) estimated $\gamma = 1.5$ from field-experiments in the river inflow of the temperate Lake Iseo. Rueda and MacIntyre (2010) estimated and modeled $\gamma = 2$ in the arctic Toolik Lake, and Cortés et al (2014a) reported values for the temperate Lake Béznar of the same order of magnitude (γ = 3-14). In our simulations, maximum mixing ratios occurred in response to increases in H, and L (northerly winds), with values that could be up to four times the median values (Fig. 6 and Table 1).

4.4 ***Time variable Ri_ρ, background $Ri_{\rho\text{-}bck}$ and the fate of river plumes in Lake Lagarfljót -*** The time variable Ri_ρ for Lagarfljót was calculated from modelled density profiles at location Lag02, of 80 m depth and 1.4 km from the inlet (see Fig. 2), representing the local conditions experienced by the river plume flowing down as a gravity current. The background Richardson number, $Ri_{\rho\text{-}bck}$, in turn, was calculated from the background density profiles (H_{bck} in Figs. 7b,c). The time-varying and background density Richardson numbers Ri_ρ and $Ri_{\rho\text{-}bck}$ for the reference and rotated-wind simulations are shown in Figs. 7d,e, together with the equilibrium intrusion depth, ID_E, calculated from the tracer experiments. The critical Ri_ρ^* was estimated as

the value of Ri_ρ below which hypolimnetic intrusions, with $ID_E > 50$ m, occurred both in the reference and the rotated-wind simulations. This estimate is ≈ 5 (Figs. 7d-e). It is O(1) and close to the value estimated from the slope-dependent parameterization proposed by Wells and Wettlaufer (2007) (their Eq. 14), where $Ri_\rho^* = 26.9304\ (\sin\theta)^{1/3}$, θ being the longitudinal slope. For the average longitudinal slope of 1.8º ($I = 0.03$) observed in Lake Lagarfljót, $Ri_\rho^* = 8.5$, which is close to our estimates from the model results.

Note that, in general, the time variable Ri_ρ is a good predictor of the fate of river inflows in the near-field. In the reference simulation, for example, Ri_ρ drops sharply at the same time as ID_E (Fig. 7d). The predictions based on Ri_ρ appears to fail in the rotated-wind simulation, during periods II and III (Fig. 10e). But note that the river densities in those periods are lower than those of the hypolimnion ($g'_{12}/\ g'_0 > 1$ in Fig. 7f). Hence, the theoretical framework presented above, only valid for $\rho_0 > \rho_2$, is not applicable and should not be used in those two periods. At any given time in the reference run (except for one period around day 258, shaded gray area in Fig. 7d), the signum of (Ri_ρ - Ri_ρ^*) and that of ($Ri_{\rho\text{-bck}}$ - Ri_ρ^*) are equal (compare the Ri_ρ(t) and $Ri_{\rho\text{-}bck}$ signals in Fig. 7d). Hence, wind-driven isopycnal displacements are not expected to cause any change in the intrusion dynamics. In response to predominantly northerly winds, the isopycnals become depressed near the inlet (it could be at times even more than twice H_{bck}, see Fig. 7b), so that Ri_ρ tends to be larger than $Ri_{\rho\text{-}bck}$. In the rotated-wind simulation, however, there are 10 periods of time when Eq. 6 holds (i.e. shaded gray areas in Fig. 7e), so that the intrusion dynamics are expected to change as a result of the isopycnal displacements. During periods I, IV, VII, IX and X in Fig. 7e, around days 206, 220, 242, 254 and 258, the isopycnals become depressed near the river inlet causing the inflows to form interflows. On day 228 (period V in Fig. 7e), in turn, the isopycnals rise and, as a result, the river plumes become underflows rather than forming metalimnetic intrusion as expected from the background density profiles. Our results, thus, demonstrate that (1) the fate of river plumes in weakly stratified environments can be, indeed, controlled by wind-driven (or free) internal oscillations causing local changes in the depth of the isopycnals, an thus in the river plume travel distances, near the inlet; and (2) this control can be parameterized, at least to first-order, in terms of a time variable density Richardson number.

385

386 4.5 ***Gravity current and displacement time scales*** – Our previous interpretation of the
387 behavior of river plumes in dynamic stratified systems, based on a time variable density
388 Richardson number, has to be taken with caution, since it is based on a theory developed for
389 stationary conditions. This approach implicitly assumes that the length of time that a tracer
390 plume takes to reach its equilibrium depth (gravity current time scale Δt_g), is much shorter than
391 the length of time during which Eq. 6 holds near the inlet (Δt_{Ri} or displacement time scale). Note
392 that the plume will disperse along the gravity current as it travels down and Δt_g should represent
393 the time for all the mass in the plume to reach its equilibrium depth. In our simulations Δt_g varied
394 from 0.5-5 days. The displacement time scale Δt_{Ri} will depend on the amplitude of the internal
395 oscillations and their period. For example, for inflows in a two-layer system subject to wind-
396 driven periodic internal oscillations where displacement ΔH(t) follows a sinusoidal behavior (see
397 details in the Appendix C), Eq. 6 will hold for a period of time given by

398

399 $$\frac{\Delta t_{Ri}}{P} = \left(1 - \frac{1}{\pi} cos^{-1}\left(\frac{Ri_{\rho}^{*} - Ri_{\rho-bck}}{Ri_{\rho-bck} \cdot f(We)}\right)\right) \quad (7)$$

400

401 Here, $P \approx 2L/(g\,(\rho_2 - \rho_1)/(\rho_2\,/(D - H_{bck}) + \rho_1/H_{bck}))^{1/2}$, is the period of internal oscillations, and D
402 is the maximum depth of the lake. The scaling function $f\,(We)$ links the thermocline
403 displacement (or wind set up) ΔH_{max} and the time-filtered Wedderburn number We (Appendix C
404 and see Shintani et al. (2010) for finite amplitude displacements). In the specific case of Lake
405 Lagarfljót, the internal oscillations fade out quickly after the wind ceases (Priet-Mahéo et al.,
406 2019), so that the isopycnal displacements are largely associated with the magnitude and
407 direction of the wind forcing. Hence, in these systems, one could also assume that the relevant
408 time scale Δt_{Ri}, to check the quasi-stationary assumption, is that of the wind forcing.
409 Independently of whether we use the internal wave or the wind forcing period as reference, if the
410 quasi-stationary assumption does not hold (i.e. $\Delta t_g \approx \Delta t_{Ri}$), the river plume will be exposed to
411 varying intrusion conditions as it travels down, and the instantaneous time varying Ri_ρ may not
412 provide a good prediction. For example, on day 240 in the reference run, one would have
413 expected underflows, instead of the modelled interflows, to develop based on the instantaneous

414 Ri_ρ being lower than Ri_ρ^* (gray arrow in Fig. 7d). However, the condition $Ri_\rho < Ri_\rho^*$ applied only
415 for less than 6 h (Δt_{Ri}), which is shorter than the time need for the plume to reach its intrusion
416 depth ($\Delta t_g \approx 24$h). Similarly, the quasi-stationary condition did not hold in Period VIII in the
417 rotated-wind run, for which $\Delta t_{Ri} < 24$ h. To overcome this limitation, we propose to use a
418 smoothed version of Ri_ρ, using a moving average-filter with a window size equal to O(Δt_g) (see,
419 as an example, the close-up view of days 240-241 in Fig. 7d).

420

421 4.6 ***Far field fate of river plumes*** – The large amplitude isopycnal displacements can affect, as
422 predicted by the time variable density Richardson number, the initial fate of river plumes in low
423 water-column stability lakes subject to strong winds such as Lake Lagarfljót. If it enters the lake
424 as an underflow, its long-term fate depends on the occurrence of physical processes capable of
425 lifting its center of mass permanently upwards. Indeed, these large amplitude wind-driven
426 isopycnal displacements are one such mechanism; the occurrence of successive underflows is
427 another. For example, a deeply intruding river plume in Lake Lagarfljót was lifted upwards by a
428 subsequent intrusion on day 261-264 (Fig. 8), after which it was transported to the shallower
429 northern shelf following northerly winds. A much stronger northerly wind event occurred on
430 days 274-275. Two deep underflows upwelled across the sill towards the shallower northern sub-
431 basin on day 276. Subject to strong wind-induced mixing and deep convectively driven
432 turbulence at night, these deep intrusions were partially incorporated into the surface mixed layer
433 and transported out of the lake by day 279. These inter-basin exchanges, driven by internal
434 oscillatory motions, are referred to, in the literature, as 'seiche pumping' (see van Senden and
435 Imboden, 1989; Lawrence et al., 1997; Laval et al. 2008). Note that the deep southern basin is
436 almost 110 m deep, the shallower northern basin is ≈ 42 m, and the sill between the two basins
437 rises to nearly 30 m of depth. Hence, the motion of deep underflows across the sill requires the
438 development of internal displacements with amplitudes of almost 70 m. This will only occur
439 under low water-column stabilities (weak stratification) and strong winds. This is frequently the
440 case in arctic systems, even at the time of the strongest density gradients in the water column
441 (see Fig. 4a). In temperate lakes, with stronger water-column stabilities compared to arctic
442 systems, these exchanges will only affect shallower metalimnetic intrusions during the
443 stratification period. However, large isopycnal displacements could still occur in response to
444 strong wind events in early spring or late fall, when the lakes are weakly stratified (e.g.,

Engelhardt and Kirillin, 2014; Pöschke et al., 2015). These two periods with weak stratification could last ~ one month each, so large isopycnal displacements, including upwelling events, could play a major role in redistributing oxygen and nutrients within the water column (e.g. Pöschke et al., 2015).

Another interesting transport mechanism to consider is the basin scale circulation associated with dominant internal wave modes. The analysis of the principal components of the hourly longitudinal velocity fields along the lake thalweg is presented in Fig. 9. The Empirical Orthogonal Functions EOFs represent the spatial structure of the dominant circulation patterns, and, their corresponding amplitudes (Principal Components PC) represent their variability in time. Note that EOFs are deviations from the time-averaged circulation in the lake. In lake Lagarfljót this average circulation highlights the asymmetry of the wind forcing (predominantly from the North), with negative velocities close to the surface and positive velocities at depths deeper than ≈ 20 m (Fig. 9a). EOF_1 corresponds to the first vertical V1H1 mode, or a two-layer flow with the top of the water column flowing in the opposite direction to the bottom (Fig. 9b). The second mode EOF_2 (Fig. 9c), in turn, represents the V2H1 mode, with two recirculation cells, and longitudinal currents from 20 to 50 m flowing in the opposite directions to the currents in the rest of the water column. These two circulation modes accounted for almost 70% of the total variance of the velocity field. The amplitudes of the first mode (PC_1, Fig. 9d) followed closely the magnitude of the wind speed along the lake axis (Fig. 9e). In addition, the time series of PC_2 lagged behind PC_1 by two days (see e.g. maximum in PC_1 on day 217 compared to PC_2 on day 219). This suggests that, as expected, the initial response of the lake to wind forcing consists of a 2-layer V1H1 mode, which rapidly evolves into a V2H1 mode. The direction of the large-scale circulation is important in controlling the velocity at which river intrusions travel horizontally from the inlet to the outlet of the lake. During persistent northerly winds (see e.g. days 233 to 250 in Fig. 9e), PC_2 was mostly negative (Fig. 9d), velocities at 20 to 50 m were directed northwards and currents at these depths travelled at a considerable speed (average values of $O(10^{-2})$ m s^{-1} Fig. 9f) towards the outlet. Consequently, in those periods, deep interflows travelled longer distances along the lake thalweg (Fig. 9f) and exited the lake faster. The northward transport of deeper interflows was, however, slowed down or arrested during periods of southerly winds, when the amplitude of the second circulation mode PC_2 was positive,

and the direction of the flow at 20 to 50 m reversed (see, for example, from day 217 to 221, or from day 252 to 260 in Figs. 9d-e).

5 Conclusions

Large-amplitude isopycnal displacements in weakly stratified lakes subject to strong winds can significantly affect the fate of negatively buoyant river plumes in the near field close to the inlet. As the mixing ratios are a function of path length from the inlet to the pycnocline, they can vary significantly depending on whether the metalimnion upwells or downwells near the inlet at the time of the inflow. Hence, if the amplitude of the displacements is sufficiently large, river inflows could be forming metalimnetic intrusions or flowing to the bottom as underflows depending on the downwelling or upwelling phase of the displacement, respectively. These switches in the intrusion dynamics, occurring in response to large amplitude isopycnal displacements near the river inlet, have been shown to occur in sub-arctic Lake Lagarfljót.

Whether or not isopycnal displacements can induce significant perturbations in the fate of river plumes in the near-field can be parameterized to a first order using a time-varying density Richardson number Ri_ρ. This dimensionless number compares the expected lake-plume density contrast at the time-varying depth of the metalimnion, after dilution, against the density difference across the metalimnion. The steady-state parameterization could be applied directly and without changes as long as the time that river plumes take to reach the metalimnion or the lake bottom (travel time) is small compared to the length of time that Eq. 6 holds. However, as the plume is advected along the bottom and disperses along the gravity current, the isopycnal positions change, and hence, different parcels in the river plume could be exhibiting different behaviors. To overcome this pitfall, it is proposed to smooth the time-varying calculations Ri_ρ using a window of size equal to the travel time of the plumes.

The far-field fate of deep underflows was significantly affected by large amplitude isopycnals displacements. On one hand, deep river plumes were found to rise almost 70 m and move to the shallower northern sub-basin across a 30 m deep sill in Lake Lagarfljót. The occurrence of successive underflows also contributes to the lifting and flushing of deep intrusions trapped in the lowest layers of the lake. On the other hand, basin scale circulation associated with a V2H1 mode produced significant metalimnetic currents $O(10^{-2})$ m s^{-1} that can

505 either accelerate or decelerate the transport time of deep metalimnetic intrusions depending upon
506 the wind direction and duration.

507 The mechanisms and processes described in this manuscript affecting the fate of river
508 plumes are expected to occur under low water column stabilities and strong wind forcings, in any
509 given lake. These conditions, though, are frequent in arctic systems during the ice-free period,
510 and even at the time of strongest stratification. In Lake Lagarfljót, river underflows are unlikely
511 to remain trapped in the deepest layers throughout the stratified period given both the regular
512 presence of internal displacements of significant amplitude, and the frequency of large inflow
513 events.

514

515 **Appendix A. Transport and mixing model of Lake Lagarfljót**

516 The lake domain was discretized using a grid with uniform cell size in the horizontal (Δx
517 $= \Delta y = 100$ m), and variable thickness in the vertical (Δz), ranging from $\Delta z = 0.5$ m near the
518 surface, to $\Delta z \approx 6$ m in the deepest layers. The lake was initially assumed quiescent with
519 horizontal isotherms and uniform suspended sediment concentration. Water temperature
520 collected on the 20th of May in 2009 at the deepest point of the lake (Hafursá in Fig. 2), with an
521 almost constant temperature of ~ 2.2 °C at all depths, was used to set the initial depth-varying
522 temperature conditions. The model was run with a 60 second time step for stability purposes.
523 Model forcings were constructed based on a data set consisting of (1) hourly wind speed and
524 direction records measured at Egilsstaðir airport to the north of the lake, and hourly air
525 temperature, pressure and relative humidity, from Hallormsstaðir in the south-eastern part of the
526 lake (Fig. 2; Icelandic Meteorological Office, 2010); (2) daily cloud cover at Svínafell (Icelandic
527 Meteorological Office, 2012) located 29 km north of the lake; (3) hourly river flow rates and
528 temperatures for the glacial river Jökulsá í Fljótsdal, non-glacial river Kelduá and water passing
529 through Kárahnjúkar power plant (Icelandic Meteorological Office, 2014); and, (4) daily
530 volumetric flow rates from Grímsá (Orkusalan, 2014). Heat flux and shear stress at the free
531 surface were estimated from the meteorological information using the same procedures as
532 outlined in Fairall et al. (1996). The light attenuation coefficient was assumed to be constant (3
533 m^{-1}) given the low resolution (monthly) of Secchi-depth measurements in the lake (~ 0.2 m) and
534 it was calculated as in Martin and McCutcheon (1998). Horizontal viscosity A_h and K_h were se to

535 0.5 $m^2 s^{-1}$. The model was forced with river discharges, temperatures and C_{SS} of the main
536 tributaries to the lake and water surface elevations at the outlet (Lagarfell in Fig. 2). Inflows from
537 the three southern tributaries converge together in the same canal 9-12 km before entering the
538 lake (Fig. 2), and they were assumed to be fully mixed. In the south end, the model domain was
539 extended to include an 8-km section of the river in order to avoid any effect of the proximity of
540 the model boundary in the fate of the southern inflows. The volumetric weighted average
541 temperature and suspended-sediment load of the three rivers were introduced in the model at the
542 upstream end of this river reach. Water temperatures in Grímsá were estimated based on a known
543 relationship with the temperature of the freshwater river Kelduá (R^2 = 0.9789, Priet-Mahéo,
544 2019).

545 The suspended sediment concentrations in the two glacial inflows (Jökulsá í Fljótsdal and
546 the outflow from the Kárahnjúkar power plant, Fig. 2) were not measured continuously during
547 the study period. For the glacial river Jökulsá í Fljótsdal the suspended sediment concentration
548 (C_{ss}, mg L^{-1}) was estimated from the daily averaged flow rates (Q, $m^3 s^{-1}$). The following
549 empirical relationship, constructed from a total number of 42 observations collected in 2004 and
550 2012 by the Icelandic Meteorological Office on behalf of the National Power Company (see
551 Þorláksdóttir and Harðardóttir, 2013, and references therein), was used:

552

553 $$C_{ss} = 22.3\ Q^{0.8732} \quad (8)$$

554

555 The high coefficient of determination (R^2 = 0.96; Priet-Mahéo, 2019) of this empirical
556 relationship suggests that our approach was, at least for this river, reasonable. The suspended-
557 sediment concentrations of water diverted from Hálslón reservoir through Kárahnjúkar dam were
558 linearly interpolated as their correlation with flow rates was not significant (R^2 <0.05, 47
559 observations). Suspended sediment concentrations in the non-glacial rivers Grímsá and Kelduá
560 are one order of magnitude lower in comparison to the glacial river inputs and were neglected.

561

Appendix B. Test for intrusion depths in a linearly stratified water body

The ability of the model to correctly represent the fate of inflows in stratified basins was tested against the experimental parameterization found in their laboratory experiments by Wells and Nadarajah (2009). In their experiments, the intrusion depth of a 2-D river plume entering a quiescent and linearly stratified water body could be parameterized as:

$$ID = (3 \pm 1)\frac{B_0^{1/3}}{N} \quad (9)$$

where B_0 is the river buoyancy flux and N is the lake buoyancy frequency. A series of synthetic simulations were conducted in a simplified bathymetry, consisting of a river channel connected to a trapezoidal basin of uniform width (= 2 km), with bottom slopes near the inlet set equal to the maximum slope observed in the southern edge of Lake Lagarfljót (= 5.7°). The lake depth and length were set to 110 m and 20 km respectively, equal to the maximum depth and the length of the main basin in Lake Lagarfljót. The lake domain was discretized using a Cartesian grid with computational cells of size $\Delta x = \Delta y = 100$ m. In the vertical direction, several grid resolutions were tested. First, a constant thickness $\Delta z = 0.5$ m was used for all layers. In the simulations with the strongest stratification, other discretizations were tested in the vertical, including a coarser uniform grid with $\Delta z = 1$, and, one with a depth-variable thickness, as used in the simulations of Lake Lagarfljót (varying from $\Delta z = 0.5$ m in the surface, increasing to ~ 6 m near the bottom; see Appendix A).

River discharge was set to 100 $m^3\ s^{-1}$ and its temperature to 11.93 °C. Lake surface temperature, T_s, was set to 22 °C in all cases (see Table 2). Different buoyancy frequencies were tested, with the theoretical intrusion depths ranging from 21 to 106 m. Table 2 shows that modeled intrusion depths lied within the range of values predicted with Eq. 9. The largest deviations encountered between the intrusion depths calculated in the numerical experiments, and the average position estimated with Eq. 9, occur for the lowest N (deepest ID). These results suggest that the current grid resolution is enough to resolve intrusion depths in the simulations conducted in Lake Lagarfljót.

Appendix C. Displacement time scale Δt_{Ri} for oscillations following a sinusoidal behavior

The time variable density Richardson number used to analyze the effect of wind forcing on the intrusion dynamics, is given by Eq. 5. If we assume that the displacement $\Delta H(t)$ follow a sinusoidal function of the form

$$\Delta H(t) = \Delta H_0 \cos\left(\frac{2\pi}{P} t\right) \tag{10}$$

where P is the internal wave period $\approx 2L/(g\,(\rho_h - \rho_e)/(\rho_h/(D - H_{bck}) + \rho_e/H_{bck}))^{0.5}$, D is the maximum depth of the lake (= 110 m), and ΔH_0 is the amplitude of the thermocline tilt driven by the wind forcing. This amplitude scales inversely with the Wedderburn number (e.g. Monismith, 1986; Shintani et al., 2010), a dimensionless parameter defined as (Thompson and Imberger, 1980)

$$We = \frac{g'_{12} {H_{bck}}^2}{u_*^2 L} \tag{11}$$

Here, L is the fetch length (= 20 km) and u_* is the friction velocity calculated as $u_* = (\tau_b\, \rho_1^{-1})^{1/2}$, from the wind shear stress τ_b. For small displacements, it can be shown that $\Delta H_0/H_{bck} = 0.5 We^{-1}$. For finite amplitude displacements (until $We \approx 1$), Shintani et al. (2010) proposed a non-linear empirical relationship, based on the arctangent of We, to predict the upwelling height ΔH_0. For $\Delta H_0/H_{bck} = We^{-1}$, it follows that the time variable Richardson number can be expressed as follows:

$$Ri_\rho(t) = Ri_{\rho-bck} + \Delta Ri_\rho \cos\left(\frac{2\pi}{P} t\right) \tag{12}$$

where the amplitude of the oscillations in Ri_ρ, ΔRi_ρ, is given by $Ri_{\rho\text{-}bck} \times f(We)$ (here we use $\Delta Ri_\rho = Ri_{\rho\text{-}bck}/We$).

From these equations, it follows that a necessary condition that need to hold for the inflow dynamics to change in response to oscillations in the near-field stratification, is that

$$Ri_{\rho-bck}\, f(We) > \left|Ri_{\rho-bck} - Ri_{\rho}^{*}\right| \quad (13)$$

Consider now, for example, the behavior of an interflow ($Ri_{\rho\text{-}bck} > Ri_{\rho}^{*}$) in a two-layer system where the thermocline exhibit oscillations that satisfy Eq. 13. The length of time in one cycle when a change in the inflow dynamics should be expected (water parcels flowing to the bottom instead of intruding at the thermocline) can be estimated by setting the condition

$$cos\left(\frac{2\pi}{P}t\right) \leq \frac{Ri_{\rho}^{*} - Ri_{\rho-bck}}{Ri_{\rho-bck} \times f(We)} \quad (14)$$

After integrating over the period P, the fraction of period when Ri_{ρ} is lower than Ri_{ρ}^{*} follows Eq. 7.

Acknowledgments

The data displayed in the figures can be accessed at https://zenodo.org/record/3776506. Financial support from the Energy Fund of the National Power Company in Iceland (Icelandic: Orkurannsóknasjóður Landsvirkjunar, P.I. Hrund Andradóttir) and the University of Iceland Research Fund (P.I. Hrund Andradóttir) is gratefully acknowledged. The Icelandic Meteorological Office, Landsvirkjun and Orkusalan are thanked for data access. Authors also thank the three anonymous reviewers for their thorough comments and suggestions.

References

Ahlfeld, D., Joaquin, A., Tobiason, A., and Mas, D. (2003), Case Study: Impact of Reservoir Stratification on Interflow Travel Time. *J. Hydraul. Eng.*, 129(12): 966-975. doi: 10.1061/(ASCE)0733-9429(2003)129:12(966).

643 Alavian, V., Jirka, G. H., Denton, R. A., Johnson, M. C., and Stefan, H. G. (1992), Density
644 Currents Entering Lakes and Reservoirs. *J. Hydraul. Eng*., 118(11):1464-1489.

645 Bournet, P.E., Dartus, D., Tassin, B., and Vinçon-Leite, B. (1999), Numerical Investigation of
646 Plunging Density Current. *J. Hydraul. Eng*. 125, 584–594. doi:10.1061/(ASCE)0733-
647 9429(1999)125:6(584)

648 Cáceres, M., Valle-Levinson, A., Sepúlveda, H. H., and Holderied, K. (2002), Transverse
649 variability of flow and density in a Chilean fjord. *Continental Shelf Research*, 22 (11-13),
650 1683-1698.

651 Carmack, E.C. (1979), Combined Influence of Inflow and Lake Temperatures on Spring
652 Circulation in a Riverine Lake. *J. Phys. Oceanogr*., 9(2), 422–434. doi:10.1175/1520-
653 0485(1979)009<0422:CIOIAL>2.0.CO;2.

654 Chen, J. C. (1980), Studies of gravitational spreading currents. Ph.D. thesis, California Institute
655 of Technology.

656 Chen, C-T. A., and Millero, F. J. (1986), Thermodynamic Properties for Natural Waters
657 Covering Only the Limnological Range. *Limnol. Oceanogr.*, 31, 657–662.
658 doi:10.4319/lo.1986.31.3.0657.

659 Chung, S., and Gu, R. (1998), Two-Dimensional Simulations of Contaminant Currents in
660 Stratified Reservoir. *J. Hydraul. Eng.*, 124(7): 704-711.

661 Cortés A., Fleenor, W. E., Wells, M. G., de Vicente, I., and Rueda, F. J. (2014a), Pathways of
662 river water to the surface layers of stratified reservoirs. *Limnology and Oceanography*, 59(1):
663 233–250. doi: 10.4319/lo.2014.59.1.0233.

664 Cortés, A., Rueda, F. J., and Wells, M. G. (2014b), Experimental observations of the splitting of
665 a gravity current at a density step in a stratified water body. *J. Geophys. Res. Oceans*, 119:
666 1038–1053. doi: 10.1002/2013JC009304.

667 Cortés, A., Wells, M. G., Fringer, O. B., Arthur, R. S., and Rueda, F. J. (2015), Numerical
668 investigation of split flows by gravity currents into two‐layered stratified water bodies, *J.*
669 *Geophys. Res. Oceans,* 120: 5254–5271. doi: 10.1002/2015JC010722.

Crochet, P., Jóhannesson, T., Jónsson, T., Sigurðsson, O., Björnsson, H., Pálsson, F., and Barstad, I. (2007), Estimating the Spatial Distribution of Precipitation in Iceland Using a Linear Model of Orographic Precipitation. *J. Hydrometeor.*, 8: 1285–1306, https://doi.org/10.1175/2007JHM795.1.

Dallimore, C. J., Hodges, B. R., and Imberger, J. (2003), Coupling an underflow model to a three-dimensional hydrodynamic model. *J. Hydraulic Eng*., 129: 748–757. doi:10.1061/(ASCE)0733-9429(2003)129:10(748).

Dallimore, C. J., Imberger, J., and Ishikawa, T. (2001), Entrainment and Turbulence in Saline Underflow in Lake Ogawara. *J. Hydraul. Eng*., 127(11): 937-948.

Ellison, T., and Turner, J. (1959), Turbulent entrainment in stratified flows. *Journal of Fluid Mechanics*, 6(3), 423-448. doi:10.1017/S0022112059000738.

Engelhardt, C., and Kirillin, G. (2014), Criteria for the onset and breakup of summer lake stratification based on routine temperature measurements. *Fundam. Appl. Limnol*., 184, 183–194. doi:10.1127/1863-9135/2014/0582.

Fairall, C. W., Bradley, E. F., Rogers, D. P., Edson, J., and Young, G. (1996), Bulk parameterization of air-sea fluxes for tropical ocean global atmosphere response experiment. *J. Geophys. Res*., 101: 3747-3764. doi: 10.1029/95JC03205.

Finger, D., Schmid, M., and Wüest, A. (2006), Effects of upstream hydropower operation on riverine particle transport and turbidity in downstream lakes. *Water Resour. Res.*, 42, W08429. doi: 10.1029/2005WR004751.

Fischer H. B., and Smith, R. D. (1983), Observations of transport to surface waters from a plunging inflow to Lake Mead. *Limnology and Oceanography*, 28 (2): 258-272. doi: 10.4319/lo.1983.28.2.0258.

Ford, D. E. and Johnson, M. C. (1983), An Assessment of Reservoir Density Currents and Inflow Processes. Technical report E-83-7. Ford, Thornton, Norton and Associates, Ltd. (for the U.S. Army Engineer Waterways Experiment Station). Vicksburg, MS.

Ford, D. E. and Johnson, L. S. (1986), An assessment of reservoir mixing processes. Technical Report E-86-7. Ford, Thornton, Norton and Associates, Ltd. (for the U.S. Army Engineer Waterways Experiment Station). Vicksburg, MS.

699 Forrest A. L., Laval, B. E., Pieters, R., and Lim, D. S. S. (2008), Convectively driven transport in
700 temperate lakes. *Limnology and Oceanography*, 53(5, part 2): 2321–2332. doi:
701 10.4319/lo.2008.53.5_part_2.2321.

702 Hallworth, M., Huppert, H., Phillips, J., and Sparks, R. (1996), Entrainment into two-
703 dimensional and axisymmetric turbulent gravity currents. *Journal of Fluid Mechanics*, 308:
704 289-311. doi:10.1017/S0022112096001486.

705 Hanna, E., Jónsson, T., and Box, J. E. (2004), An analysis of Icelandic climate since the
706 nineteenth century. *Int. J. Climatol*., 24: 1193-1210. doi:10.1002/joc.1051.

707 Hebbert, B., Patterson, J., Loh, I., and Imberger, J. (1979), Collie River Underflow into the
708 Wellington Reservoir. *Journal of the Hydraulics Division*, 105 (5): 533-545.

709 Hogg, C. A. R., Egan, G. C., Ouellette, N. T., and Koseff, J. R. (2018), Shoaling internal waves
710 may reduce gravity current transport. *Environ. Fluid Mech.* 18 (2), 383-394. doi:
711 10.1007/s10652-017-9554-8.

712 Hogg, C. A. R., Marti, C. L., Huppert, H.E., and Imberger, J. (2013), Mixing of an interflow into
713 the ambient water of Lake Iseo, *Limnology and Oceanography*, 58(2), 2013, 579–592. doi:
714 10.4319/lo.2013.58.2.0579.

715 Iceland Meteorological Office (2010), Meterorological data from Hallormsstaðir and Egilsstaðir
716 Airport. Reykjavík: Iceland Meteorological Office.

717 Iceland Meteorological Office (2012), Cloud Cover Observed at Svínafell. Reykjavík: Iceland
718 Meteorological Office.

719 Iceland Meteorological Office (2014), Water Temperatures in Lake Lagarfljót and in Jökulsá í
720 Fljótsdal. Deliveries of data from the Hydrological database, no. 2014-05-19/01 and no.
721 2014-06-12 /01.

722 Imberger, J. (1998), Flux paths in a stratified lake: A review, in J. Imberger [ed.], Physical
723 Processes in Lakes and Oceans, American Geophysical Union, pp. 1–17.

724 Imberger, J., and Patterson, J. C. (1990), Physical Limnology, Adv. Appl. Mech., 27, 303–475.

725 Jazi, S.D., and Wells, M.G. (2020), Dynamics of settling‐driven convection beneath a
726 sediment‐laden buoyant overflow: Implications for the length‐scale of deposition in lakes
727 and the coastal ocean. *Sedimentology*, 67, 699–720. doi:10.1111/sed.12660.

728 Jónsdóttir, J. F. and Uvo, C. B. (2009), Long‐term variability in precipitation and streamflow in
729 Iceland and relations to atmospheric circulation. *Int. J. Climatol.*, 29: 1369-1380.
730 doi:10.1002/joc.1781.

731 Kassem, A., Imran, J., and Khan, J. A. (2003), Three-Dimensional Modeling of Negatively
732 Buoyant Flow in Diverging Channels. *J. Hydraul. Eng*., 129(12): 936-947.
733 doi:10.1061/(ASCE)0733-9429(2003)129:12(936).

734 Laval, B. E., Morrison, J., Potts, D. J., Carmack, E. C., Vagle, S., James, C., McLaughlin, F. A.,
735 and Foreman, M. (2008), Wind-driven Summertime Upwelling in a Fjord-type Lake and its
736 Impact on Downstream River Conditions: Quesnel Lake and River, British Columbia,
737 Canada. *Journal of Great Lakes Research*, 34 (1): 189-203. doi: 10.3394/0380-
738 1330(2008)34[189:WSUIAF]2.0.CO;2.

739 Lawrence G. A., Burke, J. M., Murphy, T. P., and Prepas, E. E. (1997), Exchange of water and
740 oxygen between the two basins of Amisk Lake. *Can. J. Fish. Aquat. Sci*., 54: 2121-2132.

741 Legg, S., Hallberg, R. W., and Girton, J. B. (2006), Comparison of entrainment in overflows
742 simulated by z-coordinate, isopycnal and non-hydrostatic models. *Ocean Model*. 11, 69–97.
743 doi:10.1016/J.OCEMOD.2004.11.006.

744 Luketina, D. A., and Imberger, J. (1987), Characteristics of a surface buoyant jet. *Journal of*
745 *Geophysical Research*, 92 (C5), 5435-5447.

746 MacIntyre S., Sickman, J. O., Goldthwait, S. A., and Kling, G. W. (2006), Physical pathways of
747 nutrient supply in a small, ultraoligotrophic arctic lake during summer stratification.
748 *Limnology and Oceanography*, 51(2): 1107–1124. doi: 10.4319/lo.2006.51.2.1107.

749 Martin, J.L. and McCutcheon, S. C. (1998), Hydrodynamics and Transport for Water Quality
750 Modeling. CRC press.

751 Monismith, S. (1986), An experimental study of the upwelling response of stratified reservoirs to
752 surface shear stress. *J. Fluid Mech*. 171, 407. doi:10.1017/S0022112086001507

753 Morillo, S., Imberger, J., Antenucci, J. P., and Woods, P. F. (2008), Influence of wind and lake
754 morphometry on the interaction between two rivers entering a stratified lake. *J. Hydraulic*
755 *Eng.*, 134: 1579–1589. doi:10.1061/(ASCE)0733- 9429(2008)134:11(1579).

756 Orkusalan (2014), Grímsá River Uncorrected Temperatures. Reykjavík: Orkusalan.

757 Ouillon, R., Meiburg, E., Meiburg, E., Ouellette, N.T., and Koseff, J.R. (2019), Interaction of a
758 downslope gravity current with an internal wave. *J. Fluid Mech*., 873, 889–913.
759 doi:10.1017/jfm.2019.414.

760 Pálsson, S., and Vilmundardóttir, E. G. (2003), Classification and density of suspended solids (In
761 Icelandic: Bergflokkun og eðlismassi svifaurs), Technical Report OS-2003/059, Reykjavík:
762 Orkustofnun - Vatnamælingar.

763 Pöschke, F., Lewandowski, J., Engelhardt, C., Preuß, K., Oczipka, M., Ruhtz, T., and Kirillin, G.
764 (2015), Upwelling of deep water during thermal stratification onset-A major mechanism of
765 vertical transport in small temperate lakes in spring? *Water Resour. Res*., 51, 9612–9627.
766 doi:10.1002/2015WR017579.

767 Priet-Mahéo, M.C. (2019), Internal dynamics of a medium-sized subarctic lake: field
768 measurements and numerical modeling, PhD dissertation, Faculty of Civil and Environmental
769 Engineering, University of Iceland. https://hdl.handle.net/20.500.11815/1273

770 Priet-Mahéo, M.C., Ramón, C. L., Rueda, F. J., and Andradóttir, H.Ó. (2019), Mixing and
771 internal dynamics of a medium-size and deep lake near the Arctic circle, *Limnology and*
772 *Oceanography*, 64: 61-80. doi:10.1002/lno.11019.

773 Rueda, F. J., and MacIntyre, S. (2009), Flow paths and spatial heterogeneity of stream inflows in
774 a small multibasin lake. *Limnology and Oceanography*, 54(6): 2041-2057, doi:
775 10.4319/lo.2009.54.6.2041.

776 Rueda, F.J., and MacIntyre, S. (2010), Modelling the Fate and Transport of Negatively Buoyant
777 Storm–River Water in Small Multi-Basin Lakes. Environ. Model. Softw. 25, 146–157. doi:
778 10.1016/j.envsoft.2009.07.002.

779 Rueda F. J., and Schladow, G. (2009), Mixing and stratification in lakes of varying horizontal
780 length scales: Scaling arguments and energy partitioning. *Limnology and Oceanography*,
781 54(6): 2003-2017. doi: 10.4319/lo.2009.54.6.2003.

782 Shintani, T., de la Fuente, A., de la Fuente, A., Niño, Y., and Imberger, J. (2010),
783 Generalizations of the Wedderburn Number: Parameterizing Upwelling in Stratified Lakes.
784 *Limnol. Oceanogr.* 55, 1377–1389. doi:10.4319/lo.2010.55.3.1377.

785 Smith, P. E. (2006), A semi-implicit, three-dimensional model of estuarine circulation. Open-
786 File Report 2006-1004. USGS., Sacramento, California 2006. Available from
787 http://pubs.usgs.gov/of/2006/1004/pdf/ofr2006-1004.pdf.

788 Stevens, C. L., Hamblin, P. F., Lawrence, G. A. and Boyce, F. M. (1995), River-Induced
789 Transport in Kootenay Lake. *J. Environ. Eng.*, 121(11): 830-837.

790 Striberger, J., Björck, S., Ingólfsson, Ó., Kjær, K. H., Snowball, I., and Uvo, C. B. (2011),
791 Climate variability and glacial processes in eastern Iceland during the past 700 years based on
792 varved lake sediments. *Boreas*, 40: 28-45. doi:10.1111/j.1502-3885.2010.00153.x.

793 Tanimoto, Y., Ouellette, N. T., and Koseff, J. R. (2020), Interaction between an inclined gravity
794 current and a pycnocline in a two-layer stratification. *J. Fluid Mech.*, 887, A8.
795 doi:10.1017/jfm.2020.9.

796 Thompson, R.O.R.Y., and Imberger, J. (1980), Response of a numerical model of a stratified
797 lake to wind stress. In: Proceedings of the 2nd International Symposium of Stratified Flows,
798 Trondheim, June 1980. vol. 1, pp. 562-570.

799 Van Senden, D.C., and Imboden, D. M. (1989), Internal seiche pumping between sill-separated
800 basin. Geophys. Astrophys. *Fluid Dynamics*, 48 (1-3): 135-150.
801 doi:10.1080/03091928908219530.

802 Wells, M., and Nadarajah, P. (2009), The Intrusion Depth of Density Currents Flowing into
803 Stratified Water Bodies. *J. Phys. Oceanogr*. 39, 1935–1947. doi:10.1175/2009JPO4022.1.

804 Wells, M., and Wettlaufer, J. (2007), The long-term circulation driven by density currents in a
805 two-layer stratified basin. *Journal of Fluid Mechanics*, 572: 37-58.
806 doi:10.1017/S0022112006003478.

807 Winters, K.B., Lombard, P.N., Riley, J.J., and D'Asaro, E.A. (1995), Available potential energy
808 and mixing in density-stratified fluids. *J. Fluid Mech*. 289, 115–128.
809 doi:10.1017/S002211209500125X.

Winton, M., Hallberg, R., and Gnanadesikan, A. (1998), Simulation of Density-Driven Frictional Downslope Flow in Z -Coordinate Ocean Models. *J. Phys. Oceanogr.* 28, 2163–2174. doi:10.1175/1520-0485(1998)028<2163:SODDFD>2.0.CO;2.

Þorláksdóttir, S. B., and Harðardóttir, J. (2013), Overview of suspended sediment measurements conducted according to traditional contract with Landsvirkjun for year 2012 (In Icelandic: Yfirlit yfir svifaursmælingar sem gerðar voru samkvæmt hefðbundnum svifaurssamningum við Landsvirkjun árið 2012). Tech. rep. Nr SBTh/JHa/2013-01. Reykjavík: Iceland Meteorological Office.

821 **Table 1**. Underflow mixing ratios γ during the stratification period

	Mixing ratios		
Run	**Median**	**25th and 75th percentiles**	**Maximum value**
Reference	2.4	[1.9, 3.1]	7.5
Rotated wind	1.5	[1.3, 2.3]	6.7

822

823

824 **Table 2**. Model setup for the simulation experiments of river inflows in linearly stratified
825 systems. Theoretical intrusion depth (ID_{theory}, Eq. 9) and modeled intrusion depths (ID_{model}).

						ID_{model}		
T_s (°C)	T_b (°C)	$\Delta\rho$ (kg m^{-3})	N (Hz)	B_0 (m^2 s^{-3})	ID_{theory} (m)	Δz = 0.5 m	Δz = 1 m	Δz = 0.5-6m
22	21.7787	0.08	0.0027	8.5×10^{-4}	106.4 ± 35.5	94.0	92.9	94.7
22	21.6448	0.1	0.0030	8.5×10^{-4}	95.2 ± 31.8	86.1	-	-
22	21.5551	0.15	0.0037	8.5×10^{-4}	77.7 ± 25.9	70.0	-	-
22	21.3293	0.5	0.0067	8.5×10^{-4}	42.6 ± 14.2	36.7	-	-
22	19.6755	1	0.0095	8.5×10^{-4}	30.1 ± 10.0	25.7	-	-
22	17.0253	2	0.0143	8.5×10^{-4}	21.3 ± 7.1	17.4	-	-

826
827
828
829

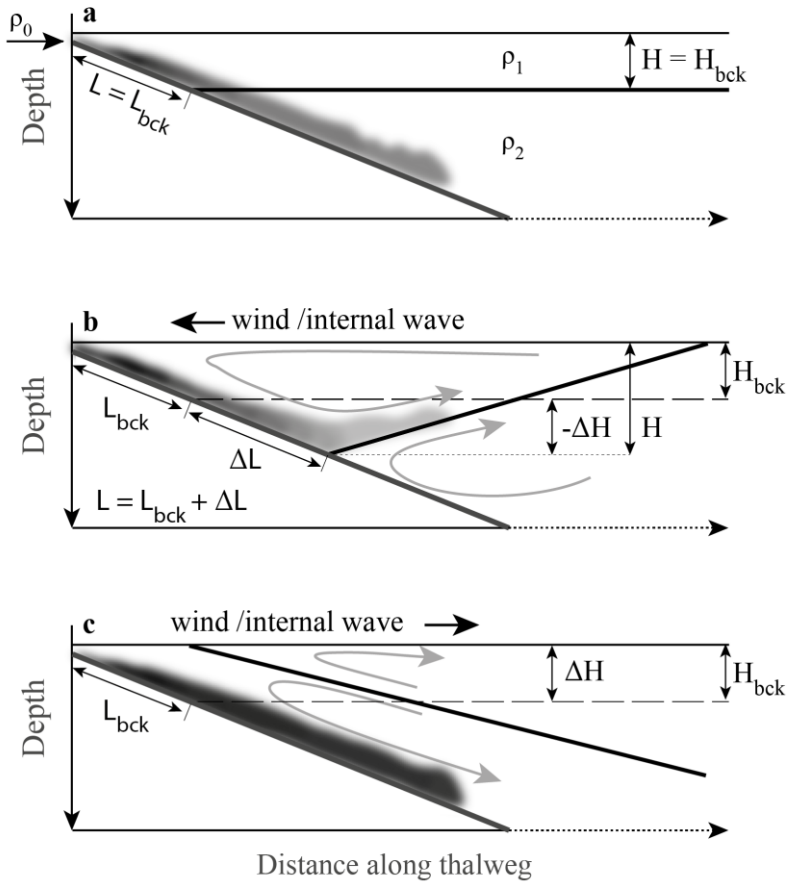

830

831 **Figure 1**. Sketches showing conceptually the location of the pycnocline (black thick line),
832 assuming a two-layer system, and mixing of a negatively-buoyant river plume (pulse or river
833 water) as it enters a lake under three different scenarios: (a) equilibrium (calm) conditions and
834 during events of (b) wind towards and (c) away from inlet, or during events of (b) downwelling
835 and upwelling phase of an internal wave. Sketches (b) and (c) are only representtive of the fate of
836 the river plume if the time needed for the plume pulse to intrude at the pycnocline or to reach the
837 bottom of the lake is shorter than the rate of change of the pycnocline position. The range of gray
838 colors represent the densitiy of the river plume, which changes as it mixes with the lake water.
839 Gray arrows in (b,c) show the V2 mode circulation in the lake. *H* is the depth of the pycnocline,
840 *L*, the distance of travel of the river plume until reaching the pycnocline, and ρ_1, ρ_2 and ρ_0
841 represent the densities of the epilimnion, hypolimnion and the river, respectively.

842

843

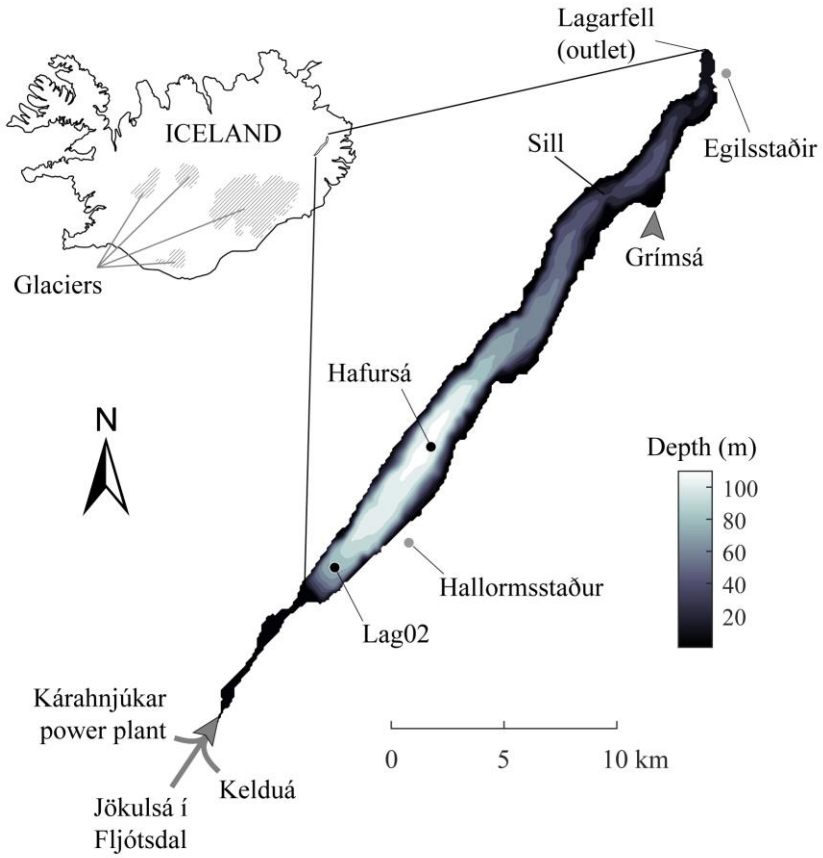

Figure 2. Lake Lagarfljót site and monitoring stations. Grey dots show the location of the two meteorological stations near the lake. Black dots match the location of two monitoring stations in the field, Lag02 and Hafursá, where a thermistor chain was deployed with an average vertical spacing between thermistors of 6 m and 7 m, respectively (details in Priet-Mahéo et al., 2019 and in Priet-Mahéo, 2019.).

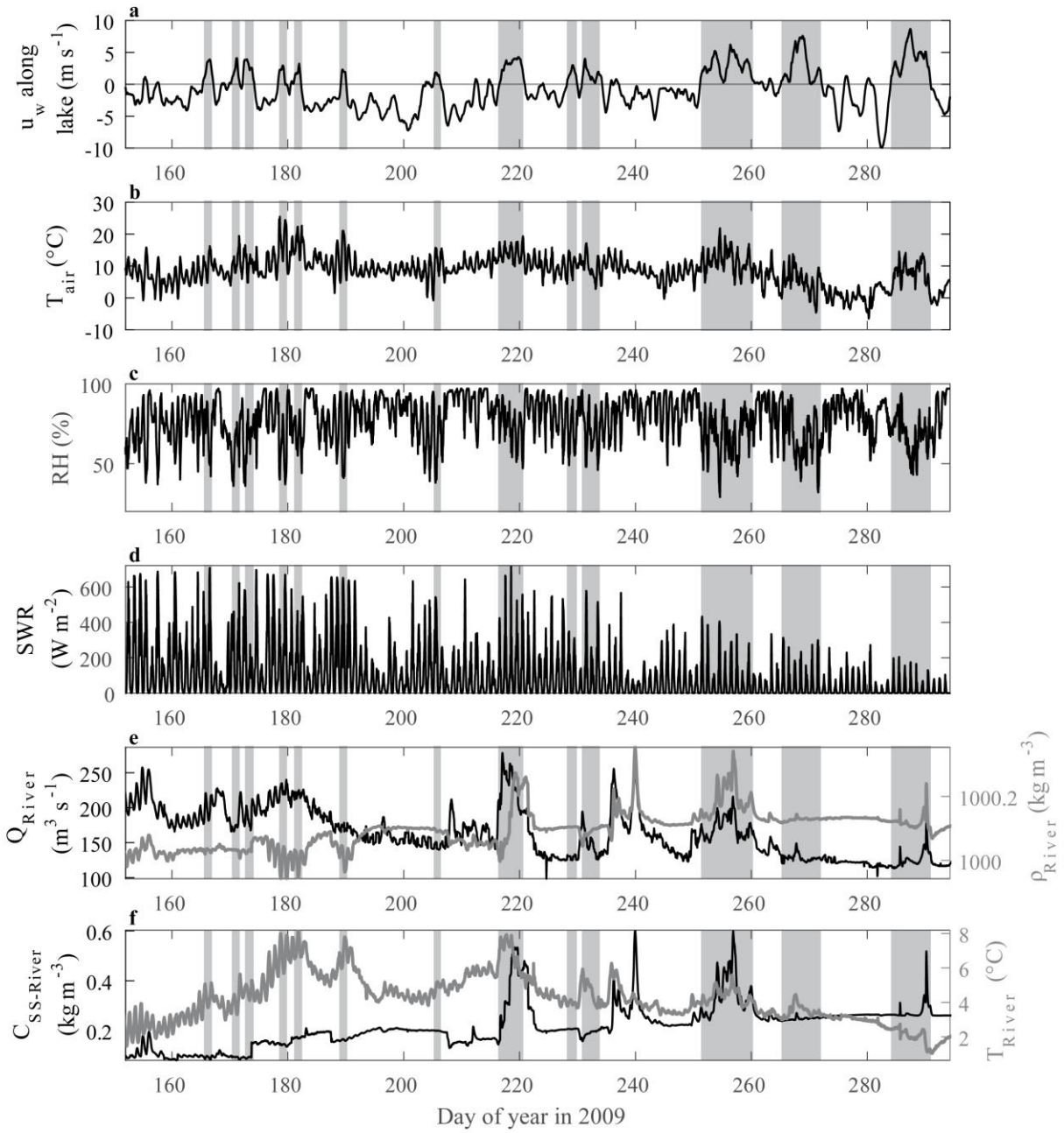

Figure 3. Hydro-meteorological forcing. (a) Wind velocity along the lake axis (smoothed over 24h), (b) air temperature (T_{air}), (c) relative humidity (RH), (d) short wave radiation (SWR), (e) discharges and density of the southern inflows, and (f) their C_{SS} and temperature. Shaded gray areas in a-f show periods of southerly-wind events.

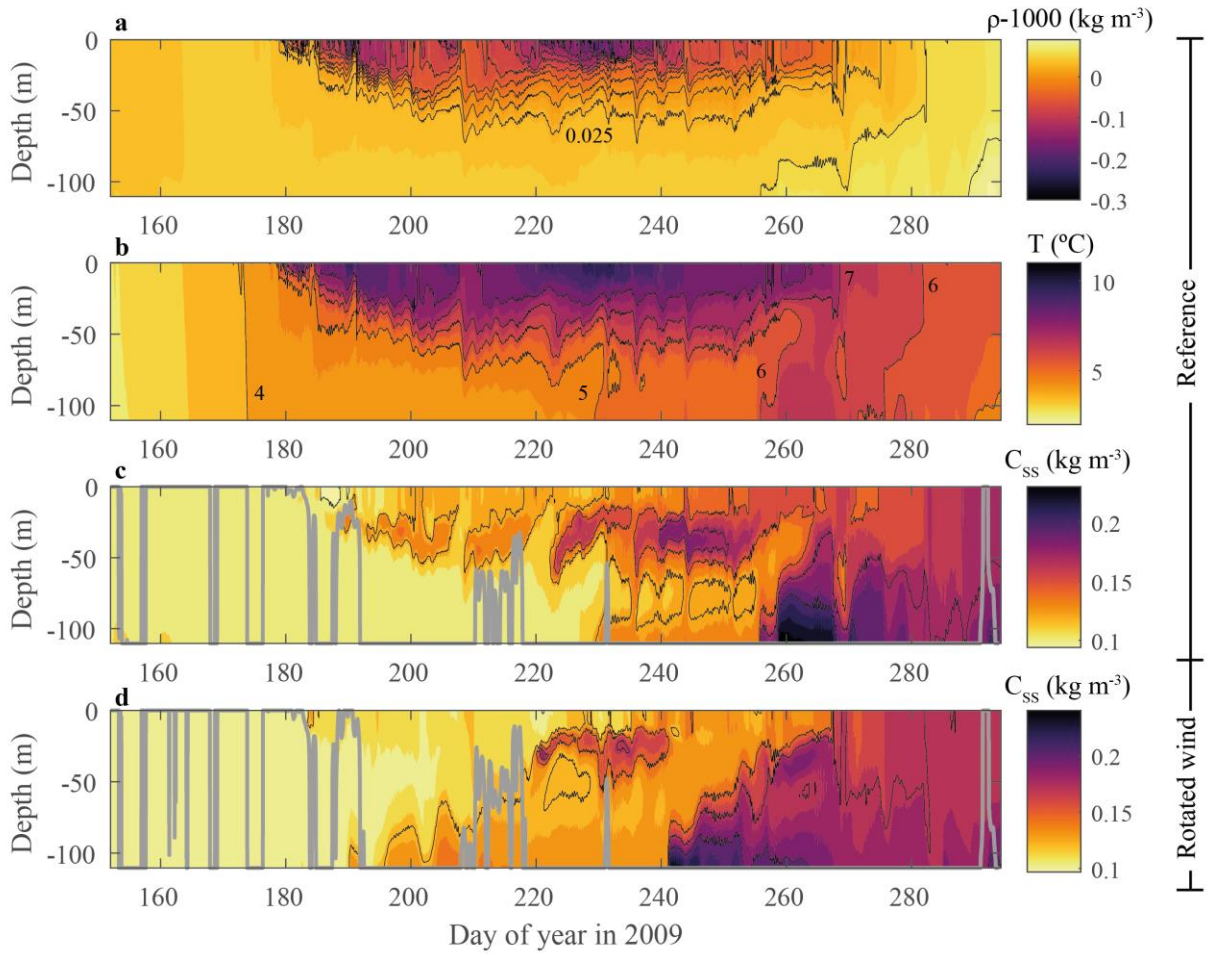

Figure 4. Stratification in Lake Lagarfljót. Modeled (a) water density anomaly, (b) temperature and (c,d) C_{SS} at Hafursá. Black lines in (a) show isopycnals with a 0.025 kg m^{-3} spacing. Solid gray lines in (c,d) show the theoretical (no mixing) intrusion depths ID_0 of the southern inflows. Results from (a-c) the reference and (d) the rotated wind simulations.

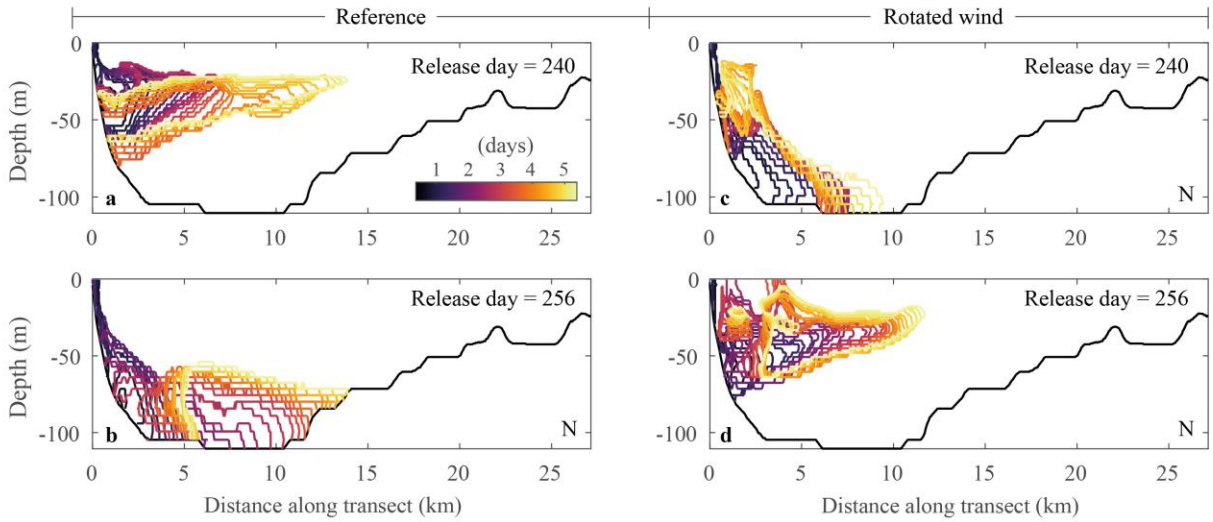

Figure 5 Spatial extent of the river plume along the lake thalweg over the first 5 days for tracer releases during the inflow events occurring on days (a,c) 240, (b,d) 256. Results from the (a,b) reference and (c,d) rotated-wind runs. Colors show the number of days from tracer release. N = north end of the lake.

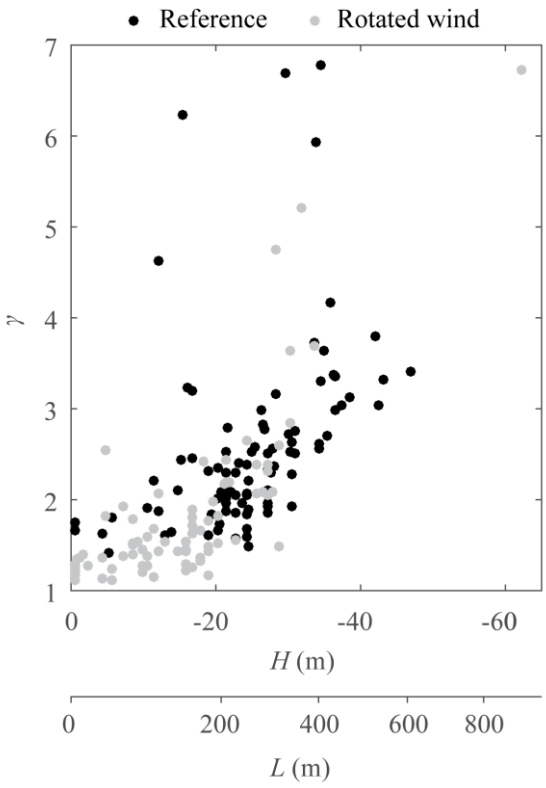

873

874 **Figure 6.** Depth of the pycnocline and travel distance L at the time of each tracer injection *vs*.
875 mixing ratios for the reference and rotated wind runs.

876
877

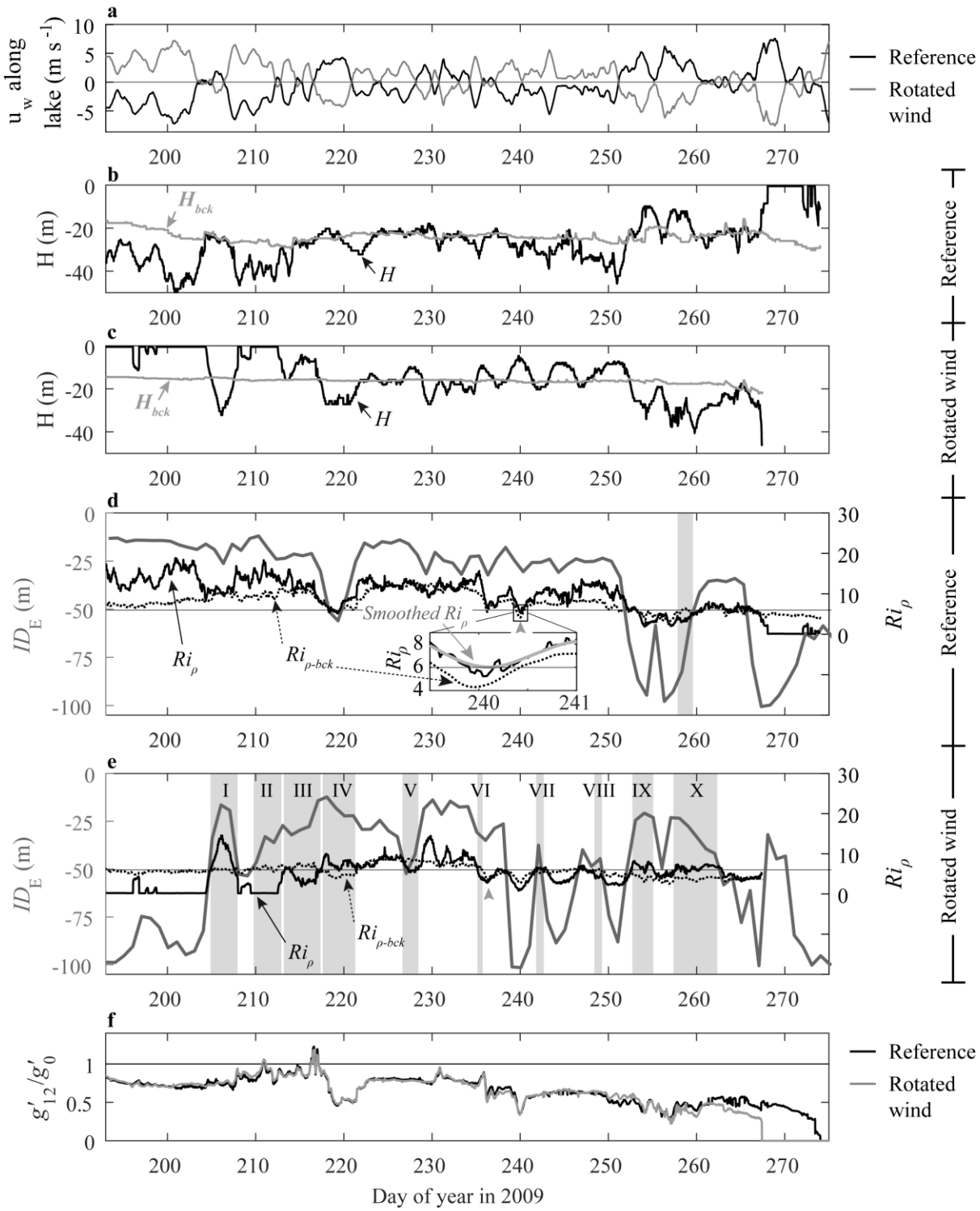

Figure 7. Fate of river plumes. (a) Wind velocity along the lake axis (smoothed over 24h) in the reference and rotated-wind simulations. (b, c) Time evolution of the pycnocline depth at Lag02 (H) and in the background profile (H_{bck}) in the reference (b) and (c) rotated wind simulations.

(d,e) Time evolution of the modeled equilibrium intrusion depths (ID_E) and density Richardson numbers calculated at Lag02 (Ri_ρ) and with the background profile ($Ri_{\rho\text{-}bck}$) in (d) the reference and (e) rotated-wind simulations. And (f) rate between the reduced gravities. The horizontal line in (d,e) marks values for ID_E = 50 m and Ri_ρ = 5. Shaded gray areas in (d,e) show times when Ri_ρ and $Ri_{\rho\text{-}bck}$ predicted the opposite fate for the river plume. Gray arrow pointers in (d,e) and the close-up view of days 240-241 in (d) show times when both Ri_ρ and $Ri_{\rho\text{-}bck}$ fail to predict the fate of the river plume. The close-up view in (d) also shows an example when interflows are correctly predicted by the smoothed Ri_ρ.

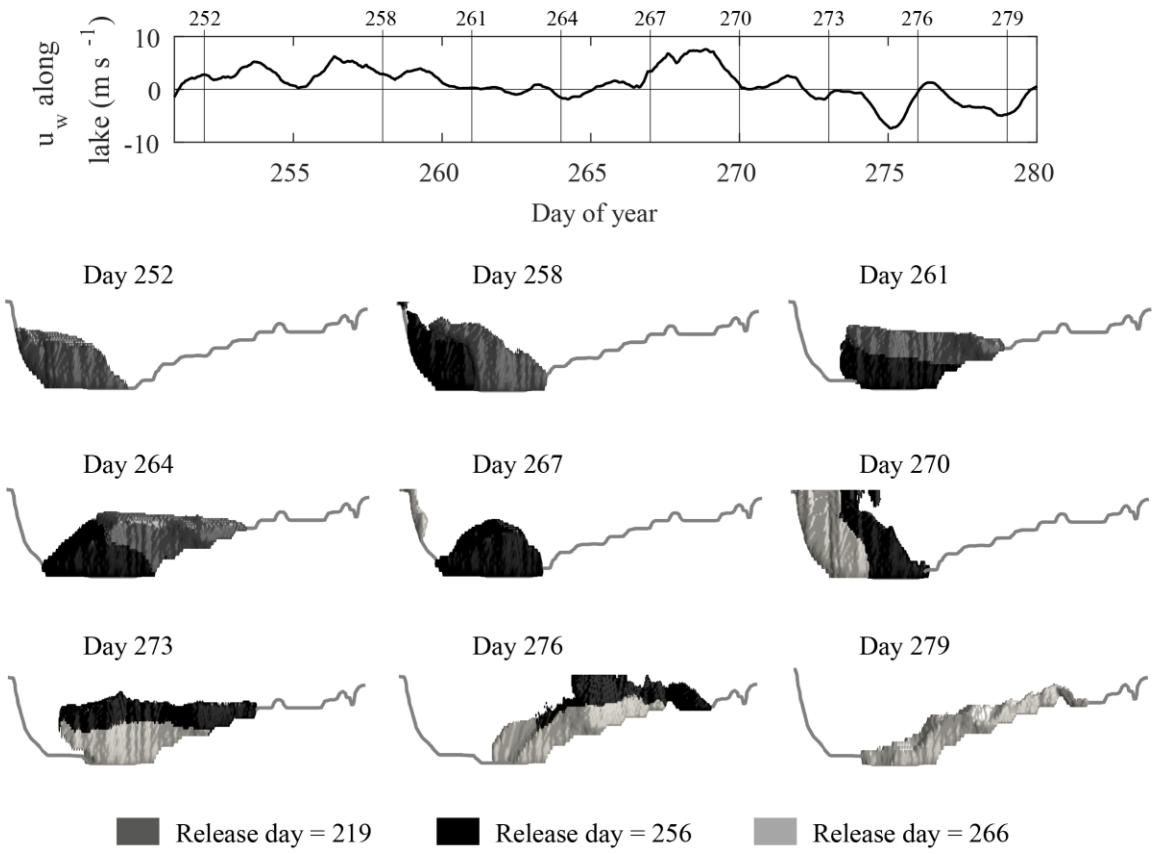

892

893 **Figure 8**. Fate of three deep underflows. The numerical tracer was released on days 219 (dark
894 grey color), 256 (black color) and 266 (light gray color), respectively, in the reference run. Plots
895 show the volume occupied by tracer concentrations > 0.05.

896
897

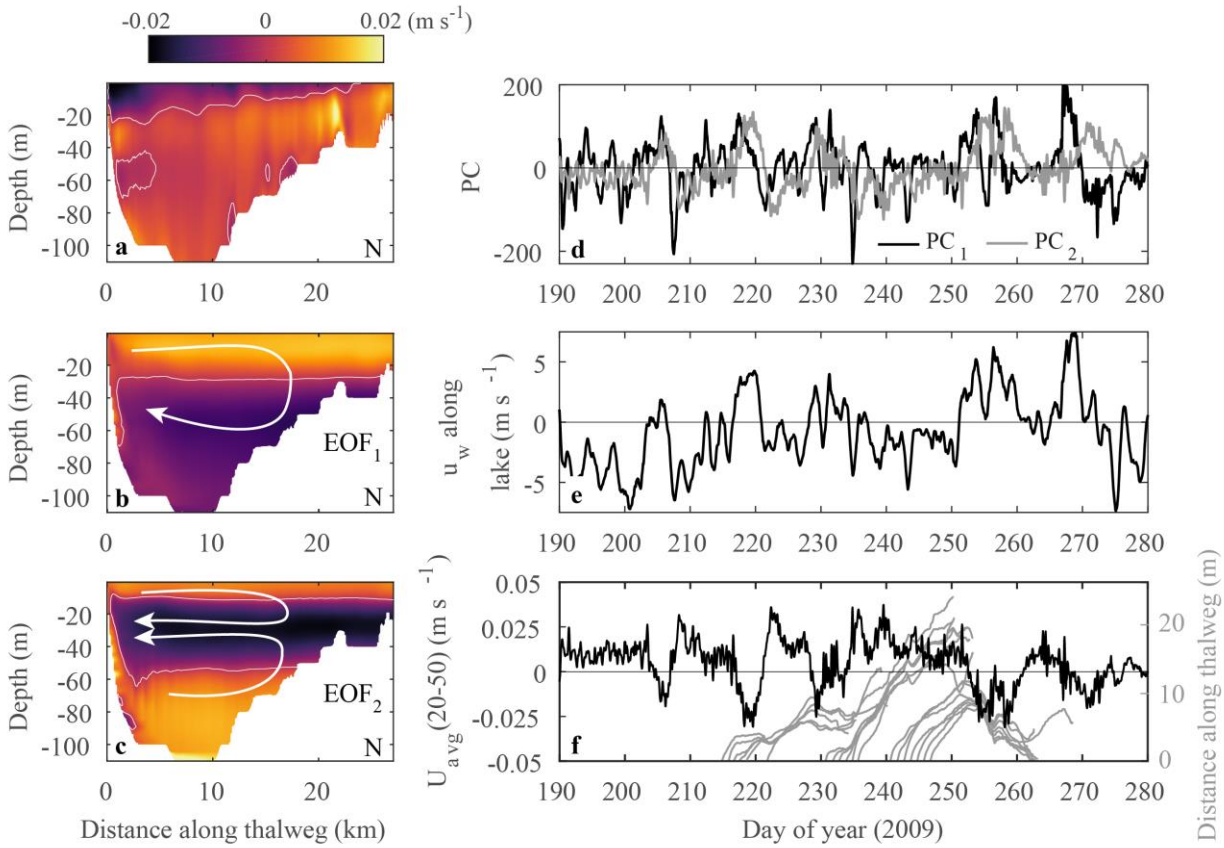

Figure 9. Effect of the basin-scale circulation on river-plume travel distances. (a) Average circulation along the lake thalweg and (b-c) modeled first two Empirical Orthogonal Functions (positive EOF_1 and EOF_2). (d) Principal components (PCs) 1 and 2. (e) Time-varying wind velocity along the lake axis (smoothed over 24h). (f) Average streamwise velocity (U_{avg}), positive if northward, between 20 and 50 m within the lake, estimated from the average circulation and the first two EOFs. And distance traveled by interflows along the lake thalweg while located at depths between 20-50 m. White lines in (a-b) show the 0 m s^{-1} isovel. Results from the reference simulation. N = north end of the lake.